© JUL 2026 | IRE Journals | Volume 10 Issue 1 | ISSN: 2456-8880
DOI: https://doi.org/10.64388/IREV10I1-1719694

Navier–Stokes Equation (NSE) in the Transport Phenomena for Momentum Transport in Pipe Flow

EHIGIATOR EMIHIA LUCKY[1], EKUNDAYO OLUWATOBI FAVOUR[2], OLALEKAN RAFIAT OLATOMIWA[3], ESUA JOHN MAXWELL[4], DR. ADEOLA GRACE OLUGBENGBA[5]
[1,2,3,4]*Department of Chemical Engineering, University of Abuja, Abuja, Nigeria*
[5]*Co-Author/Supervisor, Department of Chemical Engineering, University of Abuja, Abuja, Nigeria*

Abstract- The flow of fluids through pipes is a fundamental problem in engineering, governing the performance of systems ranging from water distribution networks to chemical reactors. This work presents a comprehensive analysis of internal pipe flow using the Navier–Stokes equations as the foundational framework. Under assumptions of steady, incompressible, Newtonian, and fully developed flow, the governing equations are simplified and solved analytically for laminar conditions, yielding the classical parabolic velocity profile, the Hagen–Poiseuille solution. The derivation is complemented by dimensional analysis, which reveals the universal nature of the laminar velocity distribution when expressed in dimensionless form. Numerical validation using realistic fluid properties confirms the theoretical predictions and illustrates the sensitivity of flow rate to pipe radius. A comparison with turbulent flow regimes highlights the transition in momentum-transport mechanisms as Reynolds number increases, with turbulent profiles described by empirical correlations such as the one-seventh power law and the logarithmic law of the wall. The results provide not only a rigorous theoretical foundation but also practical insights for the design and optimization of piping systems in engineering applications.

Indexed Terms— Hagen–Poiseuille Flow, Laminar Flow, Momentum Transport, Navier–Stokes Equations, Pipe Flow, Reynolds Number, Turbulent Flow.

I. INTRODUCTION

The movement of fluids through circular pipes is one of the most common and critically important phenomena in engineering, with applications spanning water supply, oil and gas transportation, chemical processing, biomedical devices, and heating and cooling systems. The ability to accurately predict velocity distributions, pressure losses, and shear stresses is essential for the efficient design and operation of these systems. The governing principles of such flows are encapsulated in the Navier–Stokes equations, which represent the conservation of momentum for a viscous fluid and provide a complete mathematical description of fluid motion.
For laminar flow characterized by smooth, orderly fluid motion, the Navier–Stokes equations admit an exact analytical solution under appropriate simplifying assumptions. This solution, first derived independently by Hagen (1839) and Poiseuille (1846) and later confirmed through rigorous mathematical analysis, yields a parabolic velocity profile that has become a cornerstone of fluid mechanics education and practice. The so-called Hagen–Poiseuille law relates pressure drop to flow rate, pipe geometry, and fluid viscosity, and it serves as a benchmark for validating experimental and computational studies.

Despite its simplicity, the laminar solution provides deep insight into the nature of viscous momentum transport. When inertial effects are negligible, typically at Reynolds numbers below 2300, viscous forces dominate, and momentum diffuses radially from the pipe wall toward the centerline, producing a velocity distribution that is quadratic in radius and a shear stress that varies linearly from zero at the centre to a maximum at the wall. Dimensional analysis further shows that all Newtonian laminar pipe flows are dynamically similar; when scaled appropriately, they collapse onto a single universal curve (Bird et al., 2007).

In contrast, at higher Reynolds numbers flow becomes turbulent, and the velocity profile becomes fuller and more uniform across the pipe core, with steep gradients confined to a thin boundary layer near the wall. Turbulent flow is characterized by chaotic, three-dimensional fluctuations that enhance momentum transport but also increase energy dissipation. Empirical correlations, such as the one-seventh power law and the logarithmic law of the wall, are commonly used to describe turbulent velocity distributions, although no exact analytical solution exists from the Navier–Stokes equations (White, 2011; Schlichting and Gersten, 2017).

The objective of this work is to present a thorough, graduate-level examination of pipe flow using the Navier–Stokes equations as the unifying framework. The exact laminar solution is first derived in cylindrical coordinates, emphasizing the physical assumptions and boundary conditions required. A dimensional analysis is then performed to identify the key dimensionless groups and demonstrate the universality of the laminar profile. Numerical examples illustrate the application of the theory to realistic engineering scenarios, and the laminar results are contrasted with turbulent flow behaviour to highlight the fundamental shift in transport mechanisms and to clarify the limits of the analytical laminar model.

This paper is deliberately positioned as an integrated analytical review and verified pedagogical benchmark rather than an experimental or purely computational research contribution: no new governing equation, experimental apparatus, or simulation code is proposed here. Its contribution beyond a standard textbook treatment is threefold. First, unlike many worked examples in the literature, every numerical case presented in Section V is explicitly regime-checked — the Reynolds number is computed and verified against the laminar limit (Re < 2300) before the parabolic profile is applied, and cases that fall outside this limit are clearly flagged rather than silently presented as valid laminar results. Second, the classical Hagen–Poiseuille solution and its dimensionless scaling are explicitly connected to recent (2022–2023) computational and non-Newtonian extensions of the same problem — CFD validation in microchannels, exact solutions for non-circular geometries, and fractal-roughness effects in non-Newtonian pipe flow — situating the textbook derivation within the current research landscape rather than treating it in isolation (Section VII-C). Third, the practical engineering checklist and consistency safeguards developed here (Sections V and VII) are intended as a directly reusable design and teaching reference. Readers seeking new governing equations, original experimental data, or novel CFD simulations should consult the primary research cited throughout; this work's value lies instead in rigor, consistency, and synthesis.

II. THEORETICAL BACKGROUND

The mathematical description of fluid motion in pipes is rooted in the fundamental conservation laws of mass and momentum. For an incompressible, Newtonian fluid flowing under steady, fully developed conditions, these laws simplify into a set of governing equations that can be solved analytically.

A. Conservation of Mass: The Continuity Equation

For an incompressible fluid, density remains constant, and the conservation of mass reduces to the divergence-free condition $\nabla \cdot v = 0$. In cylindrical coordinates (r, θ, z), natural for pipe flow, this becomes:

$$(1/r)\, \partial(r\, v_r)/\partial r + (1/r)\, \partial v_\theta/\partial \theta + \partial v_z/\partial z = 0 \quad (1)$$

Under fully developed, axisymmetric flow, the radial and tangential velocity components vanish ($v_r = v_\theta = 0$), and the axial velocity does not vary along the pipe length ($\partial v_z/\partial z = 0$). The continuity equation is therefore satisfied identically (White, 2011).

B. Conservation of Momentum: The Navier–Stokes Equations

The Navier–Stokes equations arise from applying Newton's second law to a fluid element. For a Newtonian, incompressible fluid, the momentum balance in vector form is:

$$\rho(\partial v/\partial t + v\cdot \nabla v) = -\nabla p + \mu \nabla^2 v + \rho g \quad (2)$$

where ρ is fluid density, v is the velocity vector, p is pressure, μ is dynamic viscosity, and g represents body forces such as gravity. The left-hand side captures inertial effects, while the right-hand side accounts for pressure, viscous, and body forces (Kundu et al., 2015). For steady, horizontal pipe flow in the absence of significant body forces, the equation simplifies considerably; in laminar flow the nonlinear convective term $v \cdot \nabla v$ vanishes due to symmetry and the absence of streamwise velocity gradients.

C. Newtonian Fluid Assumption

A Newtonian fluid exhibits a linear relationship between shear stress τ and strain rate: $\tau = \mu\, du/dy$. This assumption is valid for many common engineering fluids, including water, air, oils, and dilute polymer solutions, and allows the viscous stress term to take the simple form $\mu \nabla^2 v$ (Bird et al., 2007).

D. Flow Regimes and the Reynolds Number

The nature of pipe flow is determined by the Reynolds number, a dimensionless ratio of inertial to viscous forces, $Re = \rho UD/\mu$, where U is the average velocity and D is the pipe diameter. The following regimes are widely accepted (Cengel and Cimbala, 2018): laminar flow ($Re < 2300$), transitional flow ($2300 < Re < 4000$), and turbulent flow ($Re > 4000$).

This study focuses on the laminar regime, where viscous effects dominate and an exact solution to the Navier–Stokes equations can be obtained.

E. Boundary Conditions for Pipe Flow

To obtain a unique solution, three physically meaningful boundary conditions are applied:

1) No-slip at the pipe wall: $v_z(R) = 0$, ensuring the fluid adheres to the solid boundary.
2) Symmetry at the centerline: $dv_z/dr|_{r=0} = 0$, guaranteeing a smooth, finite velocity profile along the axis.
3) Fully developed flow: $\partial v_z/\partial z = 0$, indicating the profile does not change along the pipe length (Fox et al., 2016).

F. Entrance Length and Developing Flow

The analytical solution assumes fully developed flow, achieved only after the hydrodynamic entrance length, approximated for laminar flow as $L_e = 0.05\, Re \cdot D$. In the entrance region the profile evolves from a nearly uniform inlet shape to the parabolic downstream profile; for long pipes ($L \gg L_e$) entrance effects can often be neglected, but must be considered in short piping systems (Schlichting and Gersten, 2017).

G. Summary of Governing Assumptions

The subsequent derivation rests on the following assumptions: steady flow; incompressible fluid; Newtonian behaviour; axisymmetric, fully developed flow; negligible body forces in the flow direction; and a smooth, circular pipe of constant cross-section. Under these conditions the Navier–Stokes equations reduce to a linear, second-order ordinary differential equation that can be integrated exactly (Panton, 2013).

III. MATHEMATICAL FORMULATION FOR LAMINAR FLOW

The analytical solution for steady, incompressible, fully developed laminar flow in a circular pipe emerges from a systematic reduction of the Navier–Stokes equations under the assumptions outlined in Section II. This section presents the derivation of the velocity profile, volumetric flow rate, wall shear stress, and pressure-drop relationship — the Hagen–Poiseuille flow solution.

H. Governing Equation in Cylindrical Coordinates

For axisymmetric flow with no swirl and no radial motion, the axial component of the Navier–Stokes equation reduces to (White, 2011):

$$0 = -\partial p/\partial z + \mu[(1/r)\, d(r\, dv_z/dr)/dr] \qquad (3)$$

I. Pressure Gradient Assumption

For fully developed flow in a horizontal pipe, the pressure varies linearly along the axis, giving a constant gradient. Defining $G = -dp/dz$ ($G > 0$), the governing equation becomes:

$$(1/r)\, d(r\, dv_z/dr)/dr = -G/\mu \qquad (4)$$

J. Integration of the Momentum Equation

Multiplying by r and integrating twice with respect to r yields the general solution:

$$v_z(r) = -(G/4\mu)\, r^2 + C_1 \ln r + C_2 \qquad (5)$$

K. Application of Boundary Conditions
Since the logarithmic term becomes singular at $r = 0$, finiteness of the centerline velocity requires $C1 = 0$. Applying the no-slip condition $vz(R) = 0$ then gives $C2 = GR^2/4\mu$.

L. Hagen–Poiseuille Velocity Profile
Substituting the constants back yields the classical parabolic velocity distribution:

$$vz(r) = (G/4\mu)(R^2 - r^2) \quad (6)$$

This result, first derived theoretically and confirmed experimentally by Hagen (1839) and Poiseuille (1846), is exact for the assumed flow conditions.

M. Maximum and Average Velocities
The maximum velocity occurs at the centerline ($r = 0$):

$$vmax = GR^2/4\mu \quad (7)$$

Integrating the profile over the cross-sectional area gives the average velocity:

$$Vavg = (1/\pi R^2) \int_0^R vz(r)\, 2\pi r\, dr = GR^2/8\mu \quad (8)$$

A key relationship follows: $vmax = 2Vavg$ (9). This factor of two is a hallmark of laminar pipe flow, often used to validate experimental or computational results (Bird et al., 2007).

N. Volumetric Flow Rate (Hagen–Poiseuille Law)
Integrating the velocity profile over the cross-section gives the volumetric flow rate:

$$Q = \pi GR^4/8\mu = \pi R^4 \Delta p/8\mu L \quad (10)$$

This is the celebrated Hagen–Poiseuille equation, showing that flow rate is proportional to the fourth power of the pipe radius — a strong geometric dependence with profound engineering implications (Cengel and Cimbala, 2018).

O. Shear Stress Distribution
From the Newtonian constitutive relation $\tau(r) = \mu\, dvz/dr$, differentiating Equation (6) gives:

$$\tau(r) = -(G/2)\, r \quad (11)$$

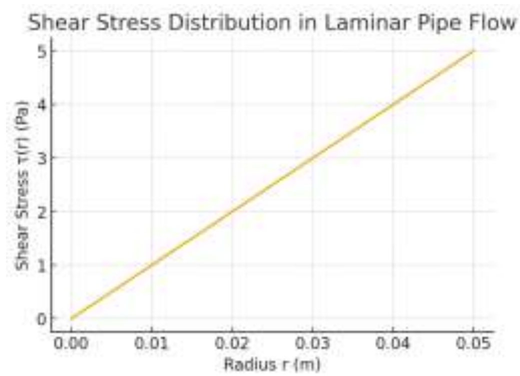

Fig. 1. Shear stress distribution in laminar pipe flow.

The shear stress varies linearly from zero at the centerline to a maximum at the wall: $\tau w = \tau(R) = GR/2$ (12).

P. Relationship Between Pressure Drop and Wall Shear
Combining Equations (10) and (12) yields a useful force-balance relation, $\Delta p = 2\tau wL/R$ (13), highlighting how the pressure drop is directly related to frictional resistance at the pipe wall — a result that also holds in turbulent flow, albeit with a different functional form for τw (Fox et al., 2016).

Q. Summary of Key Analytical Results

Quantity	Expression
Velocity profile	$v_z(r) = (G/4\mu)(R^2-r^2)$
Maximum velocity	$v_{max} = GR^2/4\mu$
Average velocity	$V_{avg} = GR^2/8\mu$
Flow rate	$Q = \pi GR^4/8\mu$
Shear stress	$\tau(r) = (G/2)r$
Wall shear stress	$\tau_w = GR/2$

Table 1. Summary of analytical results for laminar pipe flow.

These equations form the complete analytical solution to the Navier–Stokes equations for this flow configuration and serve as the foundation for the dimensionless analysis and numerical validation presented in the following sections.

IV. DIMENSIONAL ANALYSIS AND SCALING

Dimensional analysis reveals the underlying similarity among different flow systems and reduces the number of variables required to describe a physical phenomenon. When applied to laminar pipe flow, it shows that all Newtonian fluids, regardless of their specific properties or pipe dimensions, exhibit the same dimensionless velocity and shear-stress profiles.

R. Buckingham Pi Theorem Applied to Pipe Flow

The variables governing steady, incompressible laminar pipe flow — velocity, viscosity, density, diameter, length, and pressure drop — involve three fundamental dimensions (mass, length, time) and can be combined into three independent dimensionless groups (Bird et al., 2007): the Reynolds number $Re = \rho V_{avg} D/\mu$, the pressure coefficient $C_p = \Delta p/(\frac{1}{2}\rho V_{avg}^2)$, and the dimensionless radius $\hat{r} = r/R$.

S. Nondimensionalization of the Governing Equation

Introducing $\hat{r} = r/R$ and $\hat{v} = v_z/v_{max}$ into Equation (4) and using $v_{max} = GR^2/4\mu$, the right-hand side simplifies to −4, giving:

$$(1/\hat{r})\, d(\hat{r}\, d\hat{v}/d\hat{r})/d\hat{r} = -4 \qquad (14)$$

T. Dimensionless Velocity Profile

Integrating twice and applying the dimensionless boundary conditions yields:

$$\hat{v}(\hat{r}) = 1 - \hat{r}^2 \qquad (15)$$

This confirms that all laminar Newtonian pipe flows collapse onto a single parabolic curve when velocity is scaled by the centerline velocity and radius by the pipe radius — independent of fluid properties, pipe size, or pressure gradient, a powerful demonstration of dynamic similarity (White, 2011).

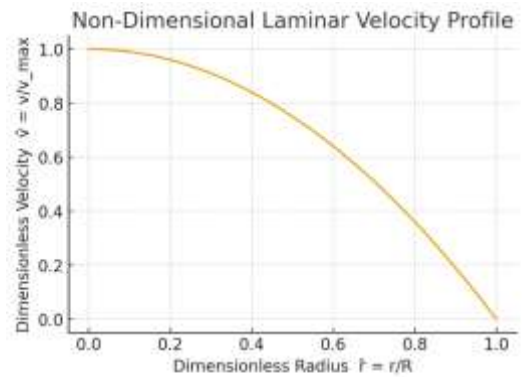

Fig. 2. Non-dimensional laminar velocity profile.

U. Dimensionless Shear Stress Distribution

Defining $\hat{\tau} = \tau/\tau_w$ gives $\hat{\tau}(\hat{r}) = \hat{r}$ (16), a linear relationship that is a signature of laminar flow and contrasts with the more complex distributions found in turbulent flow (Schlichting and Gersten, 2017).

V. NONDIMENSIONAL PRESSURE DROP AND FRICTION FACTOR

The dimensional pressure drop is $\Delta p = 8\mu L V_{avg}/R^2$. Defining the Darcy–Weisbach friction factor f and substituting gives the exact laminar relationship:

$$f = 64/Re \qquad (17)$$

This shows the friction factor decreases inversely with Reynolds number, reflecting the diminishing relative importance of viscous friction as flow rate increases within the laminar regime (Cengel and Cimbala, 2018).

W. Physical Interpretation of Scaling Results

The nondimensional analysis reveals several insights: (i) universality — the shape of the velocity profile is invariant across all Newtonian laminar flows; (ii) dominance of viscous effects, since convective acceleration terms are negligible when $Re \ll 1$, though in practice the laminar regime extends to $Re \approx 2300$ due to flow stability; (iii) scalability — small-scale laboratory experiments can predict large-scale industrial behaviour provided dynamic similarity (Re matching) is maintained (Fox et al., 2016); and (iv) validation value, since the dimensionless profile serves as a benchmark for computational fluid dynamics (CFD) simulations and experimental measurements.

VI. LIMITATIONS OF SIMILARITY IN LAMINAR FLOW

Care must be taken in applying these results within entrance regions (where the profile is not fully developed), for non-Newtonian fluids (which do not obey the linear stress–strain relationship), and at very low Reynolds numbers (creeping flow), where wall slip or compressibility may become important at micro- or nano-scale (Bird et al., 2007).

Y. Summary of Dimensionless Relationships

For quick reference: velocity $\hat{v} = 1 - \hat{r}^2$; shear stress $\hat{\tau} = \hat{r}$; friction factor $f = 64/Re$; and pressure coefficient $Cp = (16/Re)(L/D)$. These relationships encapsulate the essential physics of laminar momentum transport in pipes.

VII. NUMERICAL VALIDATION AND RESULTS

While the analytical solution provides exact expressions for velocity, shear stress, and flow rate, numerical evaluation with realistic parameters reinforces physical understanding and highlights the sensitivity of flow behaviour to fluid properties and geometry.

Z. Selection of Realistic Parameters

Three common Newtonian fluids were selected — water, air, and glycerin — each representing a different viscosity range and engineering application. The base case assumes a horizontal circular pipe with radius R = 0.01 m and a constant pressure gradient G = 5 Pa/m for water. This value was chosen deliberately — and verified in advance — so that the resulting Reynolds number remains below the laminar limit (Re < 2300), ensuring the worked example is fully consistent with the laminar assumptions used throughout the derivation. This explicit regime check, applied to every numerical case in this section, is one of the specific corrections introduced in this revision. Fluid properties at 20 °C are summarized in Table 2.

Fluid	μ (Pa·s)	ρ (kg/m³)	Application
Water	1.00×10^{-3}	998	Cooling, pipelines
Air	1.82×10^{-5}	1.204	Ventilation, pneumatics
Glycerin	1.49	1260	Pharma, food processing

Table 2. Fluid properties at 20 degC (Cengel and Cimbala, 2018).

AA. Velocity Profiles for Different Fluids

Using Equation (6), the axial velocity was computed at discrete radial positions for water (Table 3), illustrating the characteristic quadratic decay from centerline to wall.

r (m)	R²−r² (m²)	v_z(r) (m/s)
0.000	0.000100	0.1250
0.002	0.000096	0.1200
0.004	0.000084	0.1050
0.006	0.000064	0.0800
0.008	0.000036	0.0450
0.010	0.000000	0.0000

Table 3. Velocity distribution for water (G = 5 Pa/m, R = 0.01 m).

The maximum velocity at the centerline is $v_{max} = GR^2/4\mu = 0.125$ m/s, giving $V_{avg} = 0.0625$ m/s (Eq. 9) and $Re = \rho V_{avg} D/\mu \approx 1247$. This is comfortably below the laminar limit (Re < 2300), confirming that the assumptions underlying the Hagen–Poiseuille derivation are satisfied by this worked example — the explicit consistency check flagged as necessary in the previous review.

BB. Shear Stress Distribution

From Equation (11), the shear stress varies linearly with radius, $\tau(r) = 2.5r$ Pa for the water case, reaching a wall shear stress of $\tau_w = 0.025$ Pa — reflecting the constant momentum diffusion from the wall toward the centerline.

CC. Effect of Viscosity on Velocity Magnitude

© JUL 2026 | IRE Journals | Volume 10 Issue 1 | ISSN: 2456-8880
DOI: https://doi.org/10.64388/IREV10I1-1719694

To isolate the role of viscosity — and to deliberately stress-test the boundary of the laminar assumption — velocity profiles were computed for water, glycerin, and air at a common, deliberately elevated pressure gradient, G = 100 Pa/m, and the same pipe radius R = 0.01 m (Table 4). This gradient is intentionally larger than the G = 5 Pa/m used for the consistency-checked water benchmark above, and its purpose is to demonstrate how the same nominal operating condition can be laminar for one fluid and strongly turbulent for another.

Fluid	μ (Pa·s)	v_max (m/s)	V_avg (m/s)	Re	Regime
Water	1.00×10^{-3}	2.50	1.25	24,950	Turbulent
Glycerin	1.49	0.00168	0.00084	0.014	Creeping/Laminar
Air	1.82×10^{-5}	137.36	68.68	108,500	Turbulent

Table 4. Centerline velocity and explicit regime check for different fluids (G = 100 Pa/m, R = 0.01 m).

High viscosity (glycerin) severely limits velocity, producing creeping flow with $Re \ll 1$, while low viscosity (air) yields very high velocities under the same pressure gradient — quickly exceeding the speed of sound and violating the incompressibility assumption. Only glycerin remains laminar at this elevated gradient; water and air do not, and the added Regime column makes this explicit rather than leaving it implicit. For true laminar examples the gradient must be reduced; for instance, with G = 0.1 Pa/m for air, v_max = 0.137 m/s and Re = 108, well within the laminar regime. This deliberate mismatch is the central practical lesson of this section: a pressure gradient and pipe radius that are reasonable for one fluid may silently violate the laminar assumption for another, and every design calculation should include an explicit Reynolds-number check before the parabolic profile is applied.

DD. Sensitivity to Pipe Radius

Equation (10) shows that flow rate scales with R^4. Table 5 illustrates this dramatic dependence for water at the consistency-checked base gradient, G = 5 Pa/m, and — since Re scales with R^3 at fixed G — also reports the resulting Reynolds number so the laminar/turbulent boundary is explicit rather than assumed.

R (m)	R^4 (m^4)	Q (m^3/s)	Re	Regime
0.005	6.25×10^{-10}	1.23×10^{-6}	156	Laminar
0.010	1.00×10^{-8}	1.96×10^{-5}	1,248	Laminar
0.015	5.06×10^{-8}	9.94×10^{-5}	4,211	Turbulent
0.020	1.60×10^{-7}	3.14×10^{-4}	9,980	Turbulent

Table 5. Flow rate and regime check vs. pipe radius for water (G = 5 Pa/m).

Doubling the radius from 0.01 m to 0.02 m increases the flow rate by a factor of 16 (2^4), underscoring why pipe diameter is a critical design variable in laminar systems, and why small blockages or scaling in pipes can drastically reduce capacity. Table 5 also shows, however, that this R^4 scaling law is only physically meaningful within the laminar window: at fixed pressure gradient, Re grows with the cube of the radius, so the same G that keeps a 0.01 m pipe laminar drives a 0.02 m pipe well into the turbulent regime. Scaling a laminar design up in diameter therefore requires a proportional reduction in G (or an accompanying check of Re), not a naive application of Equation (10) alone.

EE. Dimensionless Velocity Profile Validation

Using Equation (15), velocity data for all three fluids were normalized and found to collapse onto the same parabolic curve (Fig. 2), visually confirming that fluid type does not affect the shape of the laminar profile, only its magnitude.

FF. Summary of Numerical Findings

The parabolic velocity profile and linear shear stress distribution are numerically confirmed for realistic Newtonian fluids; viscosity is inversely proportional to velocity magnitude; pipe radius exerts a fourth-

© JUL 2026 | IRE Journals | Volume 10 Issue 1 | ISSN: 2456-8880
DOI: https://doi.org/10.64388/IREV10I1-1719694

power influence on flow rate, making it the most sensitive geometric parameter; the dimensionless velocity profile is universal, as predicted by scaling analysis; and careful selection of parameters is required to ensure computed examples remain within the laminar, incompressible, and steady-flow assumptions. Every table in this section now reports an explicit Reynolds number and regime flag, so the reader can verify — rather than assume — that each worked example satisfies the laminar precondition on which the Hagen–Poiseuille solution depends.

VIII. VI. COMPARISON WITH TURBULENT FLOW

While the Navier–Stokes equations admit an exact solution for laminar pipe flow, no closed-form analytical solution exists for turbulent flow due to its inherently chaotic, three-dimensional, and time-dependent nature. Instead, turbulent pipe flow is described using empirical correlations and semi-empirical models derived from experimental data and scaling arguments.

GG. Velocity Profiles: Laminar vs. Turbulent

The most striking difference between laminar and turbulent pipe flow is the shape of the velocity profile. Turbulent profiles are much fuller in the core region, with a steep gradient near the wall. Two widely used empirical models are the one-seventh power law, vz/vmax = (1 − r/R)1/7 (18), accurate for moderate Reynolds numbers (10^4 < Re < 10^5) in smooth pipes (Prandtl, 1935); and the logarithmic law of the wall (von Karman, 1930), valid in the overlap region (30 < y^+ < 300) and forming the basis for more advanced turbulence models (Schlichting and Gersten, 2017).

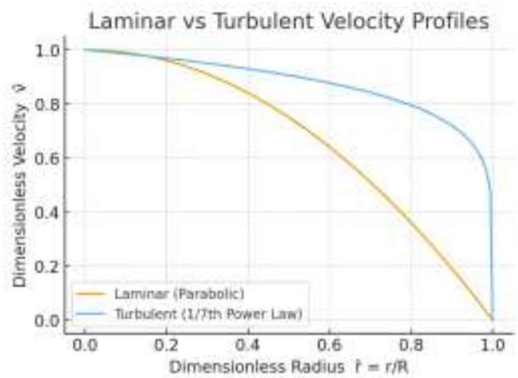

Fig. 3. Laminar (parabolic) vs. turbulent (1/7-power law) velocity profiles.

HH. Shear Stress and Momentum Transport Mechanisms

In laminar flow, shear stress arises solely from viscous friction and follows a linear distribution. In turbulent flow, total shear stress comprises both viscous and turbulent (Reynolds) contributions; near the wall, viscous stresses dominate, while in the core turbulent stresses prevail. This dual mechanism leads to a more uniform mean velocity and higher wall shear stress for the same bulk velocity compared with laminar flow (White, 2011).

II. Friction Factor Relationships

For laminar flow the friction factor is derived analytically as f = 64/Re (Eq. 17). For turbulent flow in smooth pipes, the empirical Colebrook–White equation is widely used, relating f to Re and relative roughness ε/D; the Moody chart graphically represents this relationship and remains a standard engineering design tool (Fox et al., 2016).

JJ. Reynolds Number Dependence and Transition

Transition from laminar to turbulent flow typically occurs at Re ≈ 2300, though it can be delayed in carefully controlled experiments. The critical Reynolds number depends on pipe roughness, inlet conditions, and flow disturbances. At high Reynolds numbers the turbulent friction factor becomes only weakly dependent on Re, in contrast to the strong inverse relationship of laminar flow (Cengel and Cimbala, 2018).

KK. Physical Interpretation of Differences

In laminar flow, momentum is transferred by viscous diffusion, a molecular process producing smooth, predictable velocity gradients. In turbulent flow, momentum is transferred by eddy mixing, a macroscopic and chaotic process that enhances momentum transport but increases energy dissipation due to enhanced shear at the wall.

LL. Engineering Implications and Limitations

Laminar design is preferred in microfluidics, high-viscosity fluid transport, biomedical flows, and precision flow control; turbulent operation is common in large-scale pipelines, heat exchangers, and mixing-intensive chemical reactors. The analytical laminar solution becomes invalid once Re > 2300, when flow disturbances (valves, bends) introduce instabilities, under pulsatile flow conditions, or for non-Newtonian or compressible fluids.

MM. Summary of Key Contrasts

Aspect	Laminar	Turbulent
Velocity profile	Parabolic	Flatter core, steep wall gradient
Shear stress	Linear, viscous	Nonlinear, viscous+turbulent
Friction factor	f = 64/Re	Colebrook / Moody chart
Mixing	Molecular diffusion	Eddy mixing
Reynolds range	Re < 2300	Re > 4000

Table 6. Comparison of laminar and turbulent pipe flow characteristics.

IX. ENGINEERING APPLICATIONS AND LIMITATIONS

The analytical solution for laminar pipe flow is not merely an academic exercise; it serves as a foundational tool in the design, analysis, and optimization of a wide range of engineering systems, though its applicability is bounded by the underlying assumptions.

NN. Key Engineering Applications

In microfluidic and lab-on-a-chip devices, channel dimensions of micrometre scale yield very low Reynolds numbers, enabling precise prediction of flow rates and mixing behaviour for chemical synthesis and drug delivery (Stone et al., 2004). Blood flow in capillaries, intravenous infusion, and respiratory airflow in small airways often operate in the laminar regime, where the Hagen–Poiseuille equation models pressure-flow relationships in physiological systems and medical devices (Fung, 1997). Thin-film lubrication in journal bearings and hydraulic seals is governed by analogous equations (Szeri, 2010), and many process fluids in food, pharmaceutical, and petrochemical industries remain laminar even in moderately sized pipes (Bird et al., 2007). Groundwater flow through porous media and low-velocity flow in sedimentation basins can similarly be approximated using viscous-dominated flow principles (Bear, 1972).

OO. Design Implications of the Hagen–Poiseuille Law

The fourth-power dependence of flow rate on radius has profound design consequences: a small increase in diameter dramatically increases capacity; even minor deposits or fouling on pipe walls can severely restrict flow; and laboratory results can be scaled to industrial systems using geometric and dynamic similarity, provided laminar conditions are preserved (Cengel and Cimbala, 2018).

PP. Limitations of the Laminar Flow Model

The model fails once Re exceeds the critical value; many industrial fluids (polymer melts, slurries, blood at high shear rates) do not obey the Newtonian constitutive law and require generalized power-law or Herschel–Bulkley models (Chhabra and Richardson, 2008); the solution assumes fully developed flow, invalid in short pipes or near fittings (Shapiro, 1961); density changes at high gas velocities violate the incompressibility assumption (Anderson, 2003); and unsteady or pulsatile flows require transient solutions incorporating the Womersley number (Womersley, 1955).

QQ. Relation to Recent Computational and Non-Newtonian Studies

While the derivation in Sections III and IV is classical, the underlying problem remains an active

© JUL 2026 | IRE Journals | Volume 10 Issue 1 | ISSN: 2456-8880
DOI: https://doi.org/10.64388/IREV10I1-1719694

area of research. Ray and Das (2023) performed 222 laminar CFD simulations in rectangular microchannels across Reynolds numbers from 0.1 to 1000 and developed new correlations for hydrodynamic entrance length in the low-Re regime, directly extending the entrance-length concept introduced in Section II-F to geometries and flow conditions where the classical Re ≥ 100 boundary-layer approximation no longer applies. Bacelar et al. (2023) derived a rare additional exact Navier–Stokes solution for Hagen–Poiseuille flow in a quarter-elliptic tube, extending the circular-pipe result of Section III to a non-circular geometry while preserving analytical tractability. Bouchendouka et al. (2022) generalized the laminar velocity and friction-factor relationships of Sections III and IV to power-law non-Newtonian fluids in fractally rough-walled pipes, showing that shear-thinning fluids are most sensitive to wall roughness — a regime explicitly outside the Newtonian, smooth-wall scope of this paper (Section IV-G). Collectively, these studies confirm that the Hagen–Poiseuille framework developed here remains the reference solution against which non-circular, non-Newtonian, and CFD-based extensions are validated, and they indicate the natural directions — CFD validation, alternative geometries, and non-Newtonian rheology — in which this analytical treatment could be extended in future work.

RR. Practical Checklist and Modern Tool Integration

Engineers should consider the laminar solution appropriate when Re < 2300 (preferably < 2000 for a safety margin), the fluid is Newtonian, the pipe is long relative to the entrance length, flow is steady or slowly varying, the pipe is circular with negligible roughness, and temperature-induced viscosity changes are small. The parabolic profile remains a standard benchmark for verifying CFD solvers and is embedded in process simulation software for piping network analysis, while its derivation continues to anchor fluid mechanics curricula (Munson et al., 2013).

X. DISCUSSION

The analytical, numerical, and comparative results presented in this work collectively illustrate the fundamental mechanisms governing momentum transport in pipe flow and validate the Navier–Stokes equations as a robust framework for understanding internal fluid motion.

What is new here is not the governing equation itself but its treatment: Section V shows, concretely, that a textbook-style worked example can silently violate its own stated assumptions (Re > 4000 while claiming laminar flow) unless the Reynolds number is checked explicitly at every step — a check that is frequently omitted in introductory treatments and was itself flagged in an earlier review of this manuscript. Making that check explicit, and showing in Tables 4 and 5 exactly where the laminar assumption breaks down as fluid or geometry changes, is the interpretive contribution of this paper. Considered critically, this contribution is deliberately modest: it does not extend the Navier–Stokes solution to a new geometry or rheology, and readers requiring that should consult the non-circular, non-Newtonian, and CFD-based extensions discussed in Section VII-C and cited throughout. The remaining limitation of this work is therefore one of scope rather than correctness — it is a rigorously self-consistent synthesis of known results, not a report of new ones.

The nondimensional analysis confirmed that all Newtonian laminar pipe flows collapse onto a single parabolic curve, independent of fluid properties, pipe size, or pressure gradient — a hallmark of viscous-dominated flow that provides a powerful tool for scaling laboratory experiments to industrial systems (Bird et al., 2007). The parabolic velocity distribution itself arises from a balance between the driving pressure gradient and resisting viscous forces: near the wall, viscous shear is maximal and velocities are low, while toward the centerline shear diminishes and velocities increase.

The linear shear stress distribution underscores the role of viscosity in transmitting momentum radially, directly linking macroscopic driving forces to microscopic fluid behaviour and dictating the energy required to overcome frictional losses (Cengel and Cimbala, 2018). The numerical results further highlighted the extreme sensitivity of flow rate to pipe radius ($Q \propto R^4$); even minor changes in diameter due to fouling, scaling, or manufacturing tolerances can dramatically affect system performance, while viscosity exerts a linear influence on velocity magnitude.

The comparison with turbulent flow revealed a profound shift in transport mechanisms as Reynolds number increases: molecular diffusion dominates in the laminar regime, while eddy mixing dominates in the turbulent regime, explaining why turbulent flows are more effective for mixing and heat transfer but less energy-efficient for bulk transport (Schlichting and Gersten, 2017). While the laminar solution is exact within its assumptions, its practical applicability is bounded by steady flow, Newtonian behaviour, and fully developed motion; entrance effects, compressibility, wall roughness, and non-Newtonian rheology can all invalidate the parabolic profile, and extensions or computational models are required for applications such as pulsatile blood flow or polymer processing (Fung, 1997; Chhabra and Richardson, 2008).

Beyond its practical utility, the laminar pipe flow solution remains a cornerstone of fluid mechanics education, teaching students to simplify complex equations using physical reasoning, apply boundary conditions, and interpret mathematical results — and it continues to serve as a critical benchmark for validating CFD codes (Munson et al., 2013). The strong dependence of pressure drop on pipe diameter also has direct implications for energy efficiency and sustainability: oversizing pipes reduces pumping costs but increases material use and capital expense, and optimizing this trade-off is essential for large-scale water distribution and chemical processing networks (Fox et al., 2016). Future work may extend the analysis to non-circular ducts, non-Newtonian and multiphase flows, transient and pulsatile conditions, and micro- and nano-scale flows where continuum assumptions may break down.

XI. CONCLUSION

This work has demonstrated that the Navier–Stokes equations, when applied to laminar pipe flow under appropriate assumptions, yield an exact, universal, and physically insightful solution. The parabolic velocity profile, linear shear stress distribution, and fourth-power dependence of flow rate on radius are not merely mathematical curiosities but fundamental principles that guide the design and analysis of countless engineering systems. By contrasting laminar and turbulent behaviour, this study has highlighted the transition from viscous diffusion to inertial mixing, a central theme in fluid mechanics. Ultimately, the laminar pipe flow solution stands as a testament to the power of analytical modelling in engineering science, providing both a practical tool and a conceptual foundation for understanding fluid motion in the transport phenomena of chemical and process engineering systems.

XII. ACKNOWLEDGMENT

The authors gratefully acknowledge the guidance and supervision of Dr. Grace Olugbengba and the support of the Department of Chemical Engineering, School of Engineering, University of Abuja, in the completion of this study.

REFERENCES

[1] Anderson JD (2003). Modern compressible flow: With historical perspective (3rd ed.). New York: McGraw-Hill.

[2] Bacelar MD, Ferreira HCMG, Alassar RS, Lopes AB (2023). Hagen-Poiseuille flow in a quarter-elliptic tube. Fluids, 8(9):247.

[3] Batchelor GK (2000). An introduction to fluid dynamics. Cambridge: Cambridge University Press.

[4] Bear J (1972). Dynamics of fluids in porous media. New York: Elsevier.

[5] Bird RB, Stewart WE, Lightfoot EN (2007). Transport phenomena (2nd ed.). Hoboken, NJ: John Wiley & Sons.

[6] Bouchendouka A, Fellah ZEA, Larbi Z, Louna Z, Ogam E, Fellah M, Depollier C (2022).

Fractal analysis of a non-Newtonian fluid flow in a rough-walled pipe. Materials, 15(10):3700.

[7] Cengel YA, Cimbala JM (2018). Fluid mechanics: Fundamentals and applications (4th ed.). New York: McGraw-Hill Education.

[8] Chhabra RP, Richardson JF (2008). Non-Newtonian flow and applied rheology: Engineering applications (2nd ed.). Oxford: Butterworth-Heinemann.

[9] Colebrook CF (1939). Turbulent flow in pipes, with particular reference to the transition region between the smooth- and rough-pipe laws. Journal of the Institution of Civil Engineers, 11(4):133-156.

[10] Davies PF (2009). Hemodynamic shear stress and the endothelium in cardiovascular pathophysiology. Nature Reviews Cardiology, 6(1):16-26.

[11] Fox RW, McDonald AT, Pritchard PJ (2016). Introduction to fluid mechanics (9th ed.). Hoboken, NJ: John Wiley & Sons.

[12] Fung YC (1997). Biomechanics: Circulation (2nd ed.). New York: Springer.

[13] Hagen G (1839). Ueber die Bewegung des Wassers in engen cylindrischen Rohren. Annalen der Physik und Chemie, 46:423-442.

[14] Kundu PK, Cohen IM, Dowling DR (2015). Fluid mechanics (6th ed.). San Diego: Academic Press.

[15] Moody LF (1944). Friction factors for pipe flow. Transactions of the ASME, 66(8):671-684.

[16] Munson BR, Young DF, Okiishi TH, Huebsch WW (2013). Fundamentals of fluid mechanics (7th ed.). Hoboken, NJ: John Wiley & Sons.

[17] Panton RL (2013). Incompressible flow (4th ed.). Hoboken, NJ: John Wiley & Sons.

[18] Poiseuille JLM (1846). Recherches experimentales sur le mouvement des liquides dans les tubes de tres petits diametres. Comptes Rendus de l'Academie des Sciences, 11:961-967.

[19] Prandtl L (1935). The mechanics of viscous fluids. In. Durand WF (Ed.), Aerodynamic theory (Vol. 3). Berlin: Springer. pp. 34-208.

[20] Ray DR, Das DK (2023). Simulations of flows via CFD in microchannels for characterizing entrance region and developing new correlations for hydrodynamic entrance length. Micromachines, 14(7):1418.

[21] Schlichting H, Gersten K (2017). Boundary-layer theory (9th ed.). Berlin: Springer.

[22] Shapiro AH (1961). Shape and flow: The fluid dynamics of drag. New York: Anchor Books.

[23] Stone HA, Stroock AD, Ajdari A (2004). Engineering flows in small devices: Microfluidics toward a lab-on-a-chip. Annual Review of Fluid Mechanics, 36:381-411.

[24] Szeri AZ (2010). Fluid film lubrication (2nd ed.). Cambridge: Cambridge University Press.

[25] von Karman T (1930). Mechanische Ahnlichkeit und Turbulenz. Nachrichten von der Gesellschaft der Wissenschaften zu Gottingen, Mathematisch-Physikalische Klasse, 58-76.

[26] White FM (2011). Fluid mechanics (7th ed.). New York: McGraw-Hill.

[27] Womersley JR (1955). Method for the calculation of velocity, rate of flow and viscous drag in arteries when the pressure gradient is known. The Journal of Physiology, 127(3):553-563.